

Vortex-lattice structures in rotating Bose-Fermi superfluid mixtures

Wen Wen¹, Lu Zhou^{2*}, Zhenjun Zhang¹ and Hui-jun Li^{3†}

¹ *College of Science, Hohai University, Nanjing 210098, China*

² *Department of Physics, School of Physics and Electronic Science,*

East China Normal University, Shanghai 200241, China and

³ *Institute of Nonlinear Physics and Department of Physics,*

Zhejiang Normal University, Jinhua 321004, China

(Dated: July 21, 2022)

Abstract

The system of Bose-Fermi superfluid mixture offers a playground to explore rich macroscopic quantum phenomena. In a recent experiment of Yao *et al.* [Phys. Rev. Lett. **117** 145301 (2016)], ⁴¹K-⁶Li superfluid mixture was implemented. Coupled quantized vortices are generated via rotating the superfluid mixture and a few unconventional behaviors are observed, which can be traced to boson-fermion interactions. Here we provide a theoretical insight on the unconventional behaviors of vortex lattices observed in the experiment. To this end, the orbital free density functional theory is hired, whose reliability is certificated through studying vortex lattices in strongly interacting Fermi superfluids via comparing with the full microscopic theory. We also predict interesting phenomena which can be readily explored experimentally, including the novel structures of vortex lattices in Bose-Fermi superfluid mixtures in phase separation regimes, and attractive interactions between vortices of these two superfluids.

* lzhou@phy.ecnu.edu.cn

† hjli@zjnu.cn

I. INTRODUCTION

One of the characteristic properties of superfluids is that they respond to rotation by forming quantized vortices [1]. Systems of ultracold quantum gases stand out as they provide an ideal platform to study quantized vortices with precise controls and broad tunability [2, 3]. Since the experimental realization of Bose-Einstein condensation (BEC), triangular vortex lattice being a conventional structure has been created in rotating Bose superfluids [4, 5], and widely investigated theoretically [6–8].

Meanwhile, a tunable Feshbach resonance offers a unique opportunity to access pairing and superfluidity in the crossover between a Bardeen-Cooper-Schrieffer (BCS) state of largely overlapping pairs of fermions and a BEC state of fermion dimers [9]. On the cusp of this BCS-BEC crossover, there exists a strongly interacting regime—the so-called unitary limit [10], which becomes the subject of numerous experiments [11–15]. Convincing proof of superfluidity along the BCS-BEC crossover is obtained through the observation of quantized vortices [16, 17]. In contrast to weakly interacting Bose superfluids well understood in terms of the Gross-Pitaevskii (GP) theory [6–8], a complete microscopic approach to interacting fermions is more complicated and computationally intensive [18, 19]. To account for Pauli exclusion, one should resort to the orbital-based density functional theory (DFT), such as Bogoliubov-de Gennes (BdG) equations [20–23] or superfluid local density approximation (SLDA) [24–28]. Both of the two methods require to solve a huge system of non-linear equations in a self-consistent way, and the number of the equations is on the same order as the total number of particles [20–28]. To reveal the properties and configurations of vortex lattices under experimental conditions, a spatial coarse graining of the BdG equations was performed [21]. Later on, an asymmetric SLDA was applied to study the formations of vortex lattices in spin-imbalanced unitary Fermi gases harmonically confined in two-dimensional (2D) traps [28].

While the long-sought goal of simultaneous superfluidity in mixtures of ^4He - ^3He still remains elusive due to strong interisotope interactions, Bose-Fermi superfluidity in atomic gas mixtures of ^7Li - ^6Li [29, 30], ^{41}K - ^6Li [31] and ^{174}Yb - ^6Li [32] has been realized. In a recent experiment [31], coupled vortex lattices have been created in a rotating, harmonically trapped Bose-Fermi mixture of ^{41}K - ^6Li atoms. It was observed that the boson-fermion interaction results in unusual behaviors of vortex numbers on the formations and decays of

vortex lattices. However, there is no theoretical interpretation thus far.

One can envisage that a Bose-Fermi superfluid mixture can possess novel properties of vortex lattices. Apart from the distinct quantum statistical properties of the two atom species in such a mixture, the intercomponent collision interactions alone can give rise to far richer vortex-lattice structures as compared with single-component superfluid. As in a two-component BEC [33–36], in the absence of rotation, the intercomponent interaction drives two-component BECs going through transition from miscible to immiscible phases [37]. For equal masses and equal intracomponent interactions, vortex lattices in the miscible phase have triangular, rectangular, square, and double-core structures [38, 39], while the lattices in the immiscible phase are featured by stripes and interwoven vortex sheets [39–42]. Asymmetric systems where the two components have different masses and different intracomponent interactions, support coreless vortex lattices in the miscible phase, and rotating droplets and giant skyrmions in the immiscible phase [42–44]. In addition, unequal masses can result in homogeneous infinite vortex lattices having some notable geometries [45, 46]. These studies have been focused on the somewhat less computationally intensive 2D realm.

It is thus natural to question what new features come about, if we couple a rotating, weakly interacting Bose superfluid and a rotating, strongly interacting Fermi superfluid [47–50]. Within the lowest Landau level approximation [48], the vortex lattice structures of Bose-Fermi superfluid mixtures in the BCS-BEC crossover in a rotating isotropic trap are determined by minimizing the total free energy. The core structure of a single vortex in the fermionic component of a Bose-Fermi superfluid mixture is studied by self-consistently solving the coupled BdG and GP equations [49].

The purpose of this work is to simulate the experiment [31] and present a theoretical insight on the vortex-lattice structures in a trapped three-dimensional (3D) mixture of Bose and unitary Fermi superfluids. To this end, our approach relies on the so-called orbital-free DFT [51–55], which for fermions is not written in terms of single-particle orbitals as the orbital-based DFT aforementioned, but only in terms of a single macroscopic wavefunction for the condensed state. Notably, such simplified DFT is equivalent to zero-temperature quantum hydrodynamics including the quantum pressure term [55]. The full microscopic theory, i.e. the orbital-based DFT, remains a computational challenge and requires vast computing resources for even relatively small systems, therefore experiments are too large

to be directly simulated on current computing platforms. In contrast, the orbital-free DFT provides an attractive computationally practical method for simulating huge systems under realistic conditions. By using the orbital-free DFT, the rotational properties of Bose-Fermi superfluid mixtures confined in a 2D harmonic trap [47] and in a tight toroidal trap [50] have been investigated. To demonstrate the validity of the computationally simple model, we first study the vortex configurations and the critical frequency of vortex nucleation of a single Fermi superfluid in the unitary limit, and find a remarkable qualitative agreement with those obtaining from the BdG equations [21]. Subsequently, within the orbital-free DFT, we carry out extensive numerical investigations on properties of Bose-Fermi superfluid mixtures in rotating disk-shaped traps for the experimentally relevant parameters. We study vortex-lattice structures in the miscible-immiscible phase transition by varying the repulsive boson-fermion interaction and the rotation frequency. It is found that the vortex numbers of the Bose and Fermi superfluids are strongly affected by the repulsive interspecies interaction, which are also observed in the experiment. A variety of vortex-lattice structures for various rotation frequencies in the phase-separated states are shown. This study is of particular interest in terms of the experimentally accessible conditions as it can present a comparison between the experimental results and numerical simulation of the simplified DFT, as well as illustrating some new unusual vortex formations and vortex-lattice states.

The paper is organized as follows. In Sec. II, we present the theoretical formalism for a rotating, harmonically trapped Bose-Fermi superfluid mixture, and the numerical methods used in this work. We start in Sec. III to study the properties of a single strongly interacting Fermi superfluid numerically and analytically, and compare with the microscopic theory. Next in Sec. IV, we study the effects of repulsive boson-fermion interactions on the vortex-lattice structures under various rotation frequencies. Finally, we conclude in Sec. V with a summary of our results and an outlook to future research.

II. THEORETICAL MODEL AND NUMERICAL APPROACH

We consider a mixture of a single-component bosonic superfluid and a fermionic superfluid paring between two spin components, which rotates around the z axis with the same rotation frequency Ω for both superfluids. To be close to experiments, we consider the situation of a large number of particles in realistic geometries. To find out the equilibrium vortex states of

Bose-Fermi superfluid mixtures, we use a relatively computationally simple model, i.e. the orbital-free DFT [56–60]. In terms of two complex-valued order parameters Ψ_b for condensed bosons [1] and Ψ_p for condensed fermionic pairs [61], the 3D energy functional associated with Bose-Fermi mixtures in a rotating frame of reference is written, within the mean-field approximation, as

$$E = \int \mathcal{E}[\Psi_b, \Psi_p] d\mathbf{r}, \quad (1)$$

where the energy density is

$$\begin{aligned} \mathcal{E}[\Psi_b, \Psi_p] = & \frac{\hbar^2}{2m_b} |\nabla \Psi_b|^2 + \frac{\hbar^2}{4m_f} |\nabla \Psi_p|^2 + V_b(\mathbf{r}) |\Psi_b|^2 + 2V_f(\mathbf{r}) |\Psi_p|^2 - \Psi_b^\dagger \Omega L_z \Psi_b \\ & - \Psi_p^\dagger \Omega L_z \Psi_p + \frac{1}{2} g_{bb} |\Psi_b|^4 + \frac{6}{5} \epsilon_f |\Psi_p|^2 \sigma(\eta) + g_{bf} |\Psi_b|^2 |\Psi_p|^2. \end{aligned}$$

The following calculations are performed in 3D formalism with $\mathbf{r} = \{x, y, z\}$. Here $m_b(m_f)$ is the mass of a bosonic (fermionic) atom, and $L_z = i\hbar(y\partial/\partial x - x\partial/\partial y)$ is the z component of the angular momentum. The disk-shaped trapping potentials acting on bosons and fermions are given by $V_{b,f}(\mathbf{r}) = m_{b,f}[\omega_{b\perp,f\perp}^2(x^2 + y^2) + \omega_{bz,fz}^2 z^2]/2$. The total numbers of bosonic and fermionic atoms are determined, by $N_b = \int d\mathbf{r} n_b = \int d\mathbf{r} |\Psi_b|^2$ and $N_f = \int d\mathbf{r} n_f = 2 \int d\mathbf{r} |\Psi_p|^2$, respectively.

Although it does not incorporate fermionic degrees of freedom, the orbital-free approach in Eq. (1) has computational advantage, and very recently has been used to be as a benchmark for experimental observations [11, 14, 15]. Furthermore, by comparing with the fully microscopic theory [26, 27, 62, 63], the orbital-free DFT has been proved to be a good description for static properties and low-frequency linear dynamics, in which pair-breaking effects play a negligible role [62].

The quantities g_{bb} and g_{bf} are the bosonic intraspecies and the boson-fermion interspecies interaction constants, which are related to the corresponding scattering lengths according to $g_{bb} = 4\pi\hbar^2 a_{bb}/m_b$ and $g_{bf} = 4\pi\hbar^2 a_{bf}(m_b + m_f)/(m_b m_f)$ [56]. In contrast, the strength of the two-spin fermionic interaction in the BCS-BEC crossover is characterized by the equation of state $\mu(n_f) = \partial(n_f \frac{3}{5} \epsilon_f \sigma(\eta)) / \partial n_f = \epsilon_f [\sigma(\eta) - (\eta/5) \partial \sigma(\eta) / \partial \eta]$, depending on the Fermi energy $\epsilon_f = (\hbar k_f)^2 / (2m_f)$ and the interaction parameter $\eta = 1/(k_f a_f)$, with the Fermi wave vector $k_f = (3\pi^2 n_f)^{1/3}$ and scattering length of fermions a_f . $\sigma(\eta)$ is the fitting function that is a Padé-type parametrization of the experimental data [64] for a two-component Fermi gas

at zero temperature in the BCS-BEC crossover. To obtain a further analysis, we treat the equation of state by a polytropic approximation [65, 66]

$$\mu(n_f) = \mu^0 \left(\frac{n_f}{n_0} \right)^\gamma \quad (3a)$$

$$\gamma \equiv \gamma(\eta^0) = \left(\frac{n_f}{\mu} \frac{\partial \mu}{\partial n_f} \right) |_{\eta=\eta^0} = \frac{\frac{2}{3}\sigma(\eta^0) - \frac{2\eta^0}{5}\sigma'(\eta^0) + \frac{\eta^{0^2}}{15}\sigma''(\eta^0)}{\sigma(\eta^0) - \frac{\eta^0}{5}\sigma'(\eta^0)}, \quad (3b)$$

where γ is an effective polytropic index. The reference particle number density $n_0 = (2m_f\epsilon_f^0)^{3/2}/(3\pi^2\hbar^3)$ is taken to be the density of the noninteracting Fermi gas at trap center, with the Fermi energy $\epsilon_f^0 = (\hbar k_f^0)^2/(2m_f) = \hbar(3N_f\omega_{f\perp}^2\omega_{fz})^{1/3}$, and the reference chemical potential is $\mu^0 = \epsilon_f^0[\sigma(\eta^0) - (\eta^0/5)\partial\sigma(\eta^0)/\partial\eta^0]$ with $\eta^0 = 1/(k_f^0 a_f)$ and $k_f^0 = (3\pi^2 n_0)^{1/3}$ [66].

Minimizing the energy functional with respect to variations of Ψ_b and Ψ_p , and introducing the chemical potentials μ_b and μ_p to fix the particle numbers N_b and N_f , yields the following equations

$$\mu_b \Psi_b = \left[-\frac{\hbar^2 \nabla^2}{2m_b} + V_b + g_{bb}|\Psi_b|^2 + g_{bf}|\Psi_p|^2 - \Omega L_z \right] \Psi_b \quad (4a)$$

$$\mu_p \Psi_p = \left[-\frac{\hbar^2 \nabla^2}{4m_f} + 2V_f + 2\mu(n_f) + g_{bf}|\Psi_b|^2 - \Omega L_z \right] \Psi_p, \quad (4b)$$

with $\nabla^2 = \partial^2/\partial x^2 + \partial^2/\partial y^2 + \partial^2/\partial z^2$. We introduce the energy, time and length scales, given by $\hbar\omega_{b\perp}$, $\omega_{b\perp}^{-1}$ and $\ell_{b\perp} = \sqrt{\hbar/(m_b\omega_{b\perp})}$, respectively. The order parameters are normalized by the atomic numbers in 3D as $\Psi_b \rightarrow \sqrt{N_b}\Psi_b/\ell_{b\perp}^{3/2}$ and $\Psi_p \rightarrow \sqrt{N_f/2}\Psi_p/\ell_{b\perp}^{3/2}$, and $\int d\mathbf{r}|\Psi_{b,p}|^2 = 1$. To find the stationary states of Eqs. (4), we use the imaginary time propagation of the time-dependent version of Eqs. (4) after sufficient convergence [39, 40]. The time-dependent version of Eqs.(4) takes the following dimensionless form

$$i \frac{\partial \Psi_b}{\partial t} = \left[-\frac{1}{2} \nabla^2 + \tilde{V}_b + u_b |\Psi_b|^2 + u_{fb} |\Psi_p|^2 - \tilde{\Omega} \tilde{L}_z \right] \Psi_b, \quad (5a)$$

$$i \frac{\partial \Psi_p}{\partial t} = \left[-\frac{\alpha}{2} \nabla^2 + \tilde{V}_f + u_f |\Psi_p|^{2\gamma} + u_{bf} |\Psi_b|^2 - \tilde{\Omega} \tilde{L}_z \right] \Psi_p, \quad (5b)$$

where the mass ratio is defined by $\alpha = m_b/(2m_f)$. Here the rotation frequency is $\tilde{\Omega} = \Omega/\omega_{b\perp}$ and $\tilde{L}_z = L_z/\hbar$, the trapping potentials for bosons and fermions are $\tilde{V}_b = (x^2 + y^2 + \omega_{bz}^2 z^2/\omega_{b\perp}^2)/2$ and $\tilde{V}_f = [\omega_{f\perp}^2(x^2 + y^2) + \omega_{fz}^2 z^2]/(2\alpha\omega_{b\perp}^2)$, and the dimensionless parameters for the intra- and interspecies interactions are $u_b = 4\pi N_b a_b/\ell_{b\perp}$, $u_f = 2\mu^0(N_f/2n_0\ell_{b\perp}^3)^\gamma/(\hbar\omega_{b\perp})$, $u_{fb} = 2\pi N_f m_b a_{bf}/(m_b \ell_{b\perp})$, and $u_{bf} = 4\pi N_b m_b a_{bf}/(m_b \ell_{b\perp})$, respectively.

In order to make the numerical simulation experimentally viable, we consider the parameters in the experiment by Yao *et. al.* [31], in which vortex lattices have been created

in a rotating ^{41}K - ^{6}Li superfluid mixture with an imbalanced mass $\alpha = 3.4$. The bosons and fermions fell different radial frequencies $\omega_{b\perp} = 2\pi \times 20\text{Hz}$ ($\omega_{f\perp} = 2\pi \times 40\text{Hz}$) and axial frequencies $\omega_{bz} = 2\pi \times 85\text{Hz}$ ($\omega_{fz} = 2\pi \times 237\text{Hz}$) of the disk-shaped trapping potentials. The total numbers of bosons and fermions are $N_b = 1 \times 10^4$ and $N_f = 2 \times 10^5$, respectively. To reduce the computation time, the particle numbers are both chosen to be an order of magnitude smaller than the experimental values. The scattering lengths for bosons is $a_b = 60.5a_0$ with a_0 being the Bohr radius, and the boson-fermion scattering length a_{bf} is tuned positive to study the miscibility-immiscibility transition.

Within this framework, we consider the problem by solving the two coupled nonlinear Shrödinger equations (5), with the polytropic equation of state Eq.(3a) treating exactly several important regimes of interacting Fermi superfluids. Therefore, one can study the properties of a Bose-Fermi mixture through the BCS-BEC crossover in a unified way, i.e. from a mixture of a weakly interacting Bose superfluid and a strongly interacting Fermi superfluid to a weakly interacting two-component BECs. For example, at the unitary point ($\eta^0 = 0$), the equation of state is characterized by the parameters $\mu^0 = 0.412\epsilon_f^0$ and $\gamma = 2/3$, which takes a universal density dependence $\mu^0/n_0^\gamma = 0.412\hbar^2(3\pi^2)^{2/3}/(2m_f)$ [10]. In the deep BEC regime ($\eta^0 = 6, a_f = 1168a_0$) characterized by $\mu^0 = 0.01\epsilon_f^0$ and $\gamma = 1.01$, the equation of state in terms of the above parameters takes $2\mu^0/n_0^\gamma = 0.66g_M$, slightly different from the mean-filed interaction $g_M = 4\pi\hbar^2a_M/(2m_f)$ of a BEC with the molecule-molecule scattering length $a_M = 0.6a_f$. It is because that the used equation of state includes the beyond-mean-field correction [64]. In the BEC limit ($\eta^0 = 16(70), a_M = 263(61)a_0$), the equation of state characterized by $\mu^0 = 0.004(0.0009)\epsilon_f^0$ and $\gamma = 1.003(1.0003)$ can reproduce the expected mean-field interaction $2\mu^0/n_0^\gamma = 0.9(1.0)g_M$ well.

For initial conditions, we consider the ones with a single vortex aligned with z axis at the center, modulated by a random phase at different space points [67]

$$\Psi_{b,0}(\mathbf{r}) = \left(\frac{\omega_{bz}}{\pi\omega_{b\perp}}\right)^{\frac{1}{4}} \frac{x+iy}{\sqrt{\pi}} \exp\left[-\frac{1}{2}(x^2+y^2) - \frac{\omega_{bz}}{2\omega_{b\perp}}z^2 + 2\pi i \Re(x, y)\right] \quad (6a)$$

$$\Psi_{p,0}(\mathbf{r}) = \left(\frac{\omega_{f\perp}^4 \omega_{fz}}{\alpha^5 \pi \omega_{b\perp}^5}\right)^{\frac{1}{4}} \frac{x+iy}{\sqrt{\pi}} \exp\left[-\frac{\omega_{f\perp}}{2\alpha\omega_{b\perp}}(x^2+y^2) - \frac{\omega_{fz}}{2\alpha\omega_{b\perp}}z^2 + 2\pi i \Re(x, y)\right], \quad (6b)$$

where $\Re(x, y)$ is a randomly generated number distributed uniformly between 0 and 1. The included random phase term breaks the underlying symmetries and prevents the simulation from getting stuck in any metastable states. A combination of angular harmonics with the randomly generated numbers has been successfully used to generate vortex lattices in

dipolar two-component BECs [68]. The numerical method applied is based on the split-step Crank-Nicolson scheme [69]. Vortices arrange themselves inside the trap, and the system is closer to the equilibrium configuration for long times. After each time step of computations, the wavefunctions for both superfluids are renormalized to one. Imaginary-time propagation is conducted until the desired precision is reached for the energy or chemical potential [67]. The numerical simulations are conducted in a grid with a maximum of $600 \times 600 \times 48$ points along the x , y and z directions respectively, with a spatial step of 0.1 in both x and y directions, and 0.5 in the z direction, and a time step of 0.001. To speed up the calculation, the programs are parallelized using Open Multi-processing (OpenMP) interface [70] run on supercomputing system.

III. VORTEX LATTICES IN STRONGLY INTERACTING FERMI SUPERFLUIDS

The formations of vortex lattices in a strongly interacting Fermi superfluid have been studied by using the orbital-based DFT [20, 21, 28]. In this section, we first study the properties of vortex lattices in a single Fermi superfluid, and compare our results with the previous studies based on solving the BdG equations self-consistently [21]. In Fig. 1, we present the numerical results for the vortex lattices in the unitary Fermi superfluid ($\eta^0 = 0$) as a function of the rotation frequency Ω . One can find the generated vortices from the shown cross-sectional density profiles $n_f(x, y, z = 0)$, also verified by the corresponding cross-sectional phases of the superfluids, i.e. $\arctan[\text{Im}\Psi_p(x, y, z = 0)/\text{Re}\Psi_p(x, y, z = 0)]$.

When the rotation frequency is very small, as shown in Fig. 1(a) and 1(b), a few of vortices scatter in the center, which look like point rather than hole due to the very small core radius. With increasing the rotation frequency in Fig. 1(c) and 1(d), the number of vortices gradually increases and the vortex arrays become increasingly regular. Until $\Omega = 0.95\omega_{f\perp}$ in Fig. 1(f), the edge of the Fermi superfluid filled with vortices is found to evolve from circular shape to square shape. Such square shaped edge of the rapidly rotating Fermi superfluid was first shown by calculating the BdG equations, see Fig. 1(a) of Ref. [21]. Fig. 2 illustrates the evolving of the vortex sizes and the arrangements of vortices from the strongly interacting (Fig. 2(a)) to weakly interacting Fermi superfluids (Fig. 2(b) and 2(c)), further to the weakly interacting Bose superfluid (Fig. 2(d)), with a clear transition of the

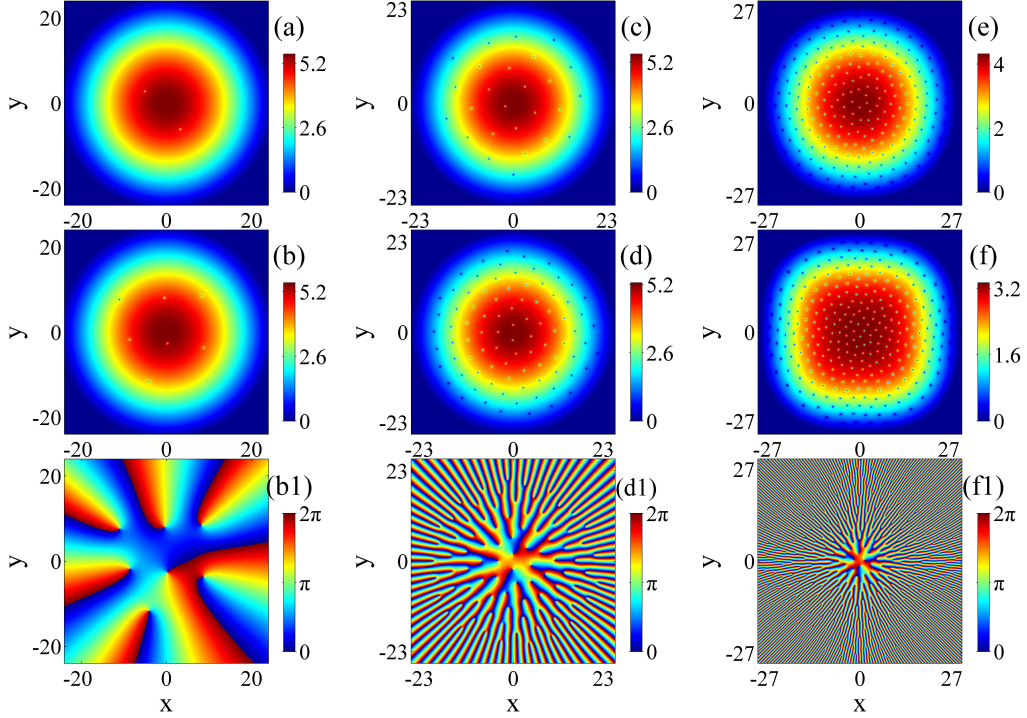


FIG. 1: The formations of vortex lattices in a strongly interacting Fermi superfluid as the rotation frequency increases: (a) $\Omega = 0.05\omega_{f\perp}$, (b) $0.075\omega_{f\perp}$, (c) $0.15\omega_{f\perp}$, (d) $0.35\omega_{f\perp}$, (e) $0.7\omega_{f\perp}$ and (f) $0.95\omega_{f\perp}$. Shown in panels (a)-(f) are the cross-sectional densities (in units of 10^{-4}) at $z = 0$ plane, and (b1), (d1) and (f1) are the corresponding cross-sectional phases.

edge shapes.

In regard to the properties of vortex lattices in a rotating strongly interacting Fermi superfluid, our first concern is the dependence of the vortex number N_v on the rotation frequency Ω . Fig. 3 shows N_v versus Ω in the different interaction regimes. In the inset, we also plot the case of the weakly interacting Bose superfluid for comparison. It is shown that the number of vortices follows a linear dependence on Ω at the low rotation frequency, and the rate of increase is larger and larger as Ω increases. However, at the large rotation frequency, when entering into the strongly interacting regimes (i.e. $\eta^0 = 0$ and 1), we find that the increase of the vortex number displays a distinctly different trend, which depends on Ω in a nonlinear way and deviates from Feynman's relation for uniform system discussed below.

At very high frequencies, a rotating superfluid mimics rigid body rotation with the average curl of the velocity field $\nabla \times \vec{v} = 2\vec{\Omega}$. The vortex density n_v obeys the Feynman's relation

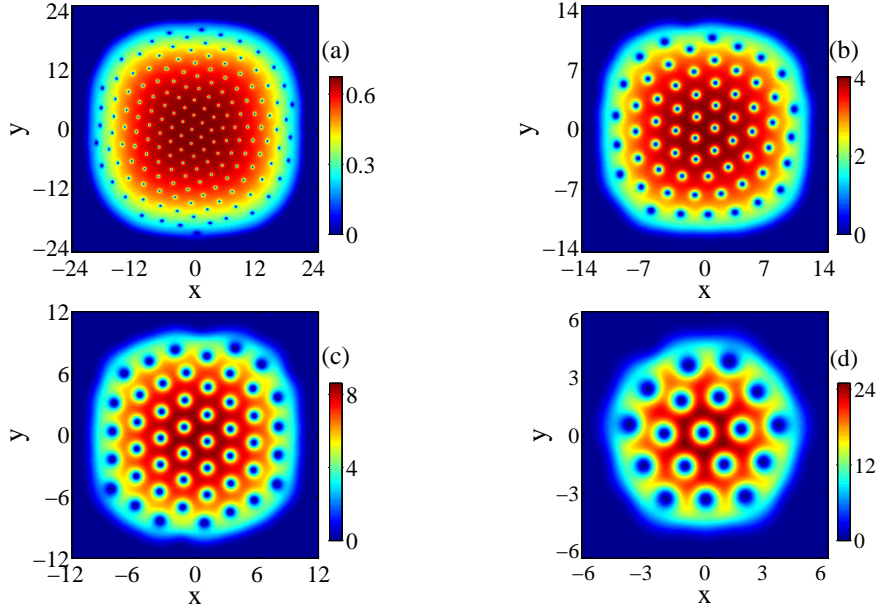


FIG. 2: Vortex lattices in the rapidly rotating Fermi superfluids for the different interaction regimes: (a) the BEC side ($\eta^0 = 1$), (b) the deep BEC regime ($\eta^0 = 16$), and (c) the BEC limit ($\eta^0 = 70$). The rotation frequency is fixed to be $\Omega/\omega_{f\perp} = 0.95$. For comparison, (d) shows the vortex lattice in the weakly interacting Bose superfluid with $\Omega/\omega_{b\perp} = 0.95$. All panels correspond to the cross-sectional densities (in units of 10^{-4}) at $z = 0$ plane.

[71]

$$n_v = \frac{2m_f\Omega}{\pi\hbar}, \quad (7)$$

which has a factor 2 for a Fermi superfluid compared with that of a Bose superfluid with the same value of atomic mass. The vortex numbers are thus given by $N_v = 4m_f/m_b(R_{f\perp}/\ell_{b\perp})^2(\Omega/\omega_{f\perp})$ for the Fermi superfluid, and $N_v = (R_{b\perp}/\ell_{b\perp})^2(\Omega/\omega_{b\perp})$ for the Bose superfluid, respectively. The radii of the superfluids containing vortices are enlarged due to the centrifugal forces, which can be estimated from the numerical results. Evaluated by the peripheral sites at which the density goes to zero from Fig. 1(f) and Fig. 2(a) for the strongly interacting regimes $\eta^0 = 0$ and 1, respectively, the radii at $\Omega = 0.95\omega_{f\perp}$ are given by $R_{f\perp}/\ell_{b\perp} = 30$ and 22. Thus the vortex numbers estimated from Feynman's theorem are $N_v = 502$ and 270, which are much larger than the numerical results $N_v = 270$ and 164 presented in Fig. 3. For the relatively weak interacting BEC regime ($\eta^0 = 6$) with $R_{f\perp}/\ell_{b\perp} = 15$ at $\Omega = 0.95\omega_{f\perp}$, the Feynman's prediction $N_v = 125$ is close to the numerical

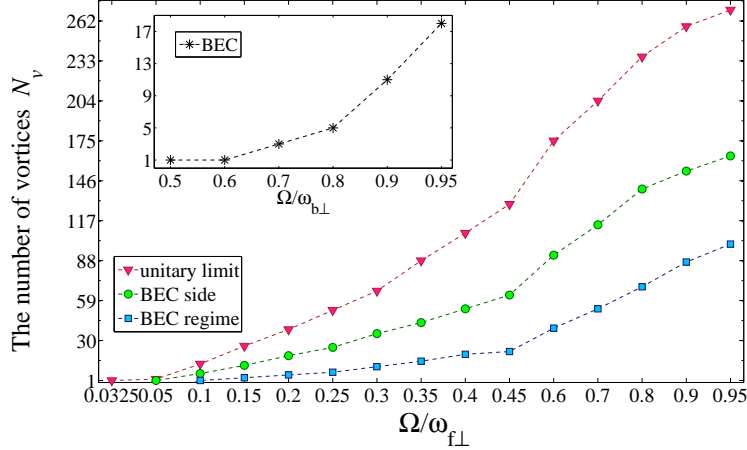


FIG. 3: The vortex numbers as a function of the rotation frequency Ω for the different interaction regimes: the unitary limit ($\eta^0 = 0$), the BEC side ($\eta^0 = 1$), and the BEC regime ($\eta^0 = 6$). Inset: the behavior of the vortex number in the weakly interacting Bose superfluid.

result $N_v = 100$. Moreover, for the weakly interacting Bose superfluid, the numerical result of $N_v = 18$ at $\Omega = 0.95\omega_{b\perp}$ shown in the inset of Fig. 3 agrees well with Feynman's theorem $N_v = 19$, which is determined by $R_{b\perp}/\ell_{b\perp} = 4.5$ evaluated from Fig. 2(d).

In Ref. [21], the vortex number $N_v = 137$ of the unitary Fermi superfluid with $\Omega = 0.8\omega_{f\perp}$ is obtained by solving the BdG equations. The calculated value from the microscopic theory is less than our result $N_v = 236$ as shown in Fig. 3. This can be traced to that the microscopic theory can account for the filling of fermionic vortex cores with a normal component [24, 28, 74], even at zero-temperature. Our formulation in terms of the order parameter can only model the superfluid, but miss the normal state. As a result, a vanishing order parameter yields a vanishing density [63, 72], which overestimates the density contrast of the vortex core, and leads to exaggerated vortex number.

The second concern is the critical frequency Ω_c of the vortex nucleation in the strongly interacting Fermi superfluids [73, 74]. The thermodynamic critical frequency can be calculated as $\Omega_c = (E_1 - E_0)/\langle L_z \rangle$ analytically, where E_1 and E_0 are the energy of the single-vortex state and the vortex-free energy, respectively, and $\langle L_z \rangle$ is the mean angular momentum of a vortex state. We have previously obtained the extra energy for per unit length of a uniform Fermi system [72], with a single quantum of circulation lying long the axis of a cylinder of radius $R_{f\perp}$. Dividing the extra energy by the angular momentum yields the characteristic

frequency of the first vortex nucleation

$$\Omega_c = \frac{\hbar}{2m_f R_{f\perp}^2} \ln(1.464\gamma^{\frac{2}{5}} \frac{R_{f\perp}}{\xi_f}), \quad (8)$$

with the Thomas-Fermi (TF) radius $R_{f\perp} = \sqrt{2\mu_f/(2m_f\omega_{f\perp}^2)}$ and the coherence length $\xi_f = \hbar/\sqrt{4m_f\mu_f}$ evaluated by the central density. They are both determined by the chemical potential $\mu_f = \hbar\omega_{b\perp}[\omega_{fz}(\omega_{f\perp}^2/(2\alpha\omega_{b\perp}))^{\frac{3}{2}}u_f^{\frac{1}{\gamma}}\Gamma(\frac{1}{\gamma} + \frac{5}{2})/(\omega_{f\perp}\Gamma(\frac{1}{\gamma} + 1)\pi^{\frac{3}{2}})]^{2\gamma/(2+3\gamma)}$ of the Fermi superfluid. In the BEC limit ($\gamma = 1$), Eq. (8) can reproduce the result $\Omega_c = \hbar/(m_b R_{b\perp}^2) \ln(1.464 R_{b\perp}/\xi_b)$ of the Bose superfluid, with $R_{b\perp} = \sqrt{2\mu_b/(m_b\omega_{b\perp}^2)}$, $\xi_b = \hbar/\sqrt{2m_b\mu_b}$, and $\mu_b = \hbar\omega_b[15u_b\omega_{bz}/(16\sqrt{2}\pi\omega_{b\perp})]^{5/2}$.

For our chosen parameters, the critical frequencies from Eq.(8) are given by $\Omega_c = \{0.016, 0.03, 0.06\}\omega_{f\perp}$ in the unitary limit ($\eta^0 = 0$), the BEC side ($\eta^0 = 1$) and the BEC regime ($\eta^0 = 6$), respectively, which are a little smaller than the numerical results $\Omega_c = \{0.0325, 0.05, 0.1\}\omega_{f\perp}$ (see Fig. 3). The numerical simulations are larger than the analytical results for a uniform system in a rotating cylinder of radius, this is due to that the nonuniform density in the axisymmetric trap reduces the total angular momentum relative to that of a uniform system. As an example, the critical frequency of the Bose superfluid can enhance from $\Omega_c = 0.2\omega_{b\perp}$ to $\Omega_c = 5\hbar/(2m_b R_{b\perp}^2) \ln(0.671 R_{b\perp}/\xi_b) = 0.42\omega_{b\perp}$ by considering inhomogeneity [1], which is in good agreement with the numerical result $\Omega_c = 0.5\omega_{b\perp}$ (see the inset of Fig. 3). The monotonic increase of the critical frequency from the unitary limit to the BEC side of the crossover is also found by solving the BdG equations [21], and the critical frequency $\Omega_c = 0.069\omega_{f\perp}$ in the unitary limit is reported. The larger value obtained from the microscopic theory can again be traced to the normal component.

IV. IMPACT OF THE BOSON-FERMION INTERACTION

After a test of the orbital-free DFT and the numerical procedures to the formations of vortex lattices in the unitary Fermi superfluids, we next investigate the effects of repulsive boson-fermion interactions on the rotating Bose-Fermi superfluid mixtures, focusing on the unitary limit ($\eta^0 = 0$) in the experimentally accessible ranges. In order to evaluate the strength of the repulsive boson-fermion interaction, in Fig. 4 we present the density distributions of nonrotating Bose and Fermi superfluids ($\Omega = 0$) for various boson-fermion interactions. As a reference, we introduce a dimensionless scattering length $\tilde{a}_{bf} = a_{bf}/(60.9a_0)$

scaled by the scattering length studied in the experiment [31]. A relevant characteristic of

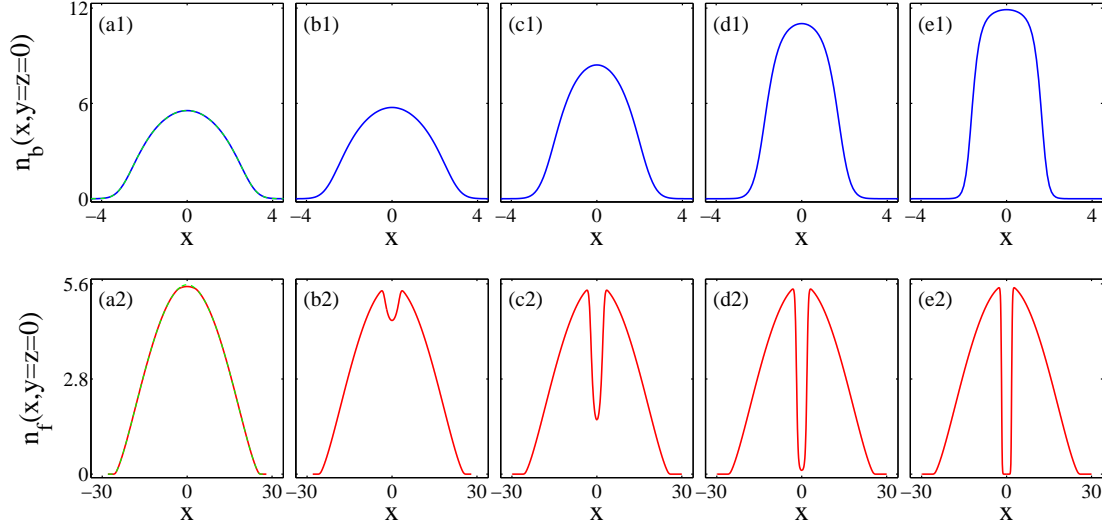


FIG. 4: The nonrotating densities of the Bose (upper panels, in units of 10^{-2}) and Fermi (lower panels, in units of 10^{-4}) superfluids as a function of x , with increasing the boson-fermion scattering length from (a) $\tilde{a}_{bf} = a_{bf}/(60.9a_0) = 0.05$, (b) 1.0, (c) 3.0, (d) 4.0 to (e) 6.0. The densities of the Bose and Fermi superfluids without the interaction ($\tilde{a}_{bf} = 0$) are also drawn as dashed lines in panels (a1) and (a2), respectively, for comparison.

coupled mixtures is the miscibility of the components [75]. In the miscible phase, the densities of two components overlap with each other; whereas, they get spatially separated in immiscible phase. For a weak repulsive interspecies interaction ($\tilde{a}_{bf} = 0.05$) in Fig. 4(a), it is shown that the density distributions of the Bose and Fermi superfluids are almost identical to the uncoupled densities ($\tilde{a}_{bf} = 0$) denoted by the dashed lines. Increasing the repulsive interaction ($\tilde{a}_{bf} = 1$) in Fig. 4(b) which is for the experimental case, the density of the Fermi superfluid reduces at the center pronouncedly, but the mixture is still overlapping in the miscible phase. Further increasing the interaction ($\tilde{a}_{bf} = 6$) in Fig. 4(e) to induce immiscibility transition, there is a shell structured geometry, in which the bosonic atoms occupy the small central region as the core-part, and the density of the fermions is zero at the center forming the large shell-part.

A parameter to measure the spatial overlapping between densities of the components can

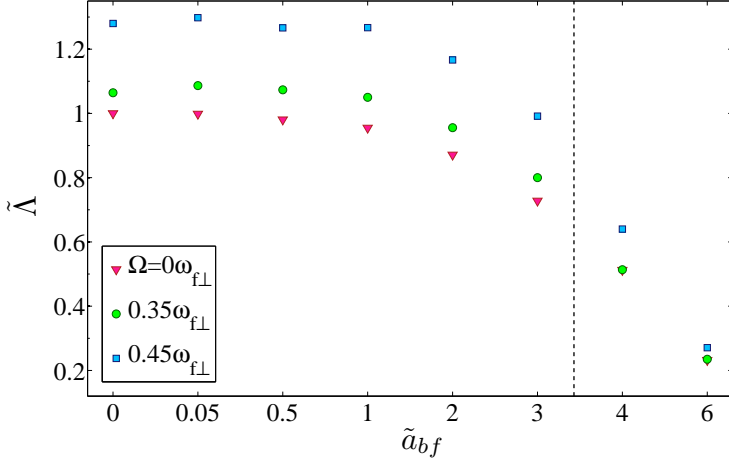


FIG. 5: The scaled overlap parameter $\tilde{\Lambda} = \Lambda/\Lambda_0$ of the Bose-Fermi superfluid mixture as a function of \tilde{a}_{bf} for various rotation frequencies. The value $\Lambda_0 = 0.135$ is for the case without interspecies interaction ($\tilde{a}_{bf} = 0$) and rotation ($\Omega = 0$). The analytical prediction $\tilde{a}_{bf} = 3.4$ of the miscible-immiscible transition without rotation is marked with the vertical dashed line.

be given by

$$\Lambda = \int d\mathbf{r} \sqrt{|\Psi_b|^2 |\Psi_p|^2}, \quad (9)$$

where the order parameters Ψ_b and Ψ_p are both normalized to one. Even without interspecies interaction, the overlap parameter in our case is merely up to $\Lambda_0 = 0.135$. We have a smaller value of $\Lambda = 0.129$ for $\tilde{a}_{bf} = 1$, indicating partial overlapping for the ratio $\tilde{\Lambda} = \Lambda/\Lambda_0 = 0.95$. Fig. 5 shows the scaled overlap parameter $\tilde{\Lambda}$ as a function of \tilde{a}_{bf} . One can find the system undergoes a miscible-immiscible transition in the parameter range of $\tilde{a}_{bf} = 3 \sim 4$ corresponding to $\Lambda = 0.1 \sim 0.07$.

The energy density of a homogenously mixed phase of the Bose-Fermi superfluid mixture can be obtained from Eq. (1) by neglecting the kinetic energy terms, that is $\mathcal{E}_r = 3\hbar^2(3\pi^2)^{\frac{2}{3}}n_f^{\frac{5}{3}}\sigma(\eta)/(10m_f) + g_{bb}n_b^2/2 + g_{bf}n_bn_f/2$. A condition for miscibility is that the Hessian matrix of \mathcal{E}_r is positive semidefinite [76], i.e. $(\partial^2\mathcal{E}_r/\partial n_b^2)(\partial^2\mathcal{E}_r/\partial n_f^2) - (\partial^2\mathcal{E}_r/\partial n_b\partial n_f)^2 > 0$. The solution of this inequality gives the parameter regime of boson-fermion scattering length

$$a_{bf}^2 < \frac{3m_{bf}^2 a_{bb} (3\pi^2)^{\frac{2}{3}}}{10\pi m_b m_f} \frac{\partial^2}{\partial n_f^2} [n_f^{\frac{5}{3}} \sigma(\eta)], \quad (10)$$

where the homogeneous mixed phase is energetically stable. In the unitary limit $\sigma(\eta)$ is taken as the universal factor $\xi = 0.41$ [64], and n_f is approximated by the Fermi density at

the trap center without the interspecies interaction. For our chosen parameters, the critical value for miscibility of the Bose and Fermi superfluids is estimated as $\tilde{a}_{bf}^c = 3.4$, which is denoted by the vertical dashed line in Fig. 5.

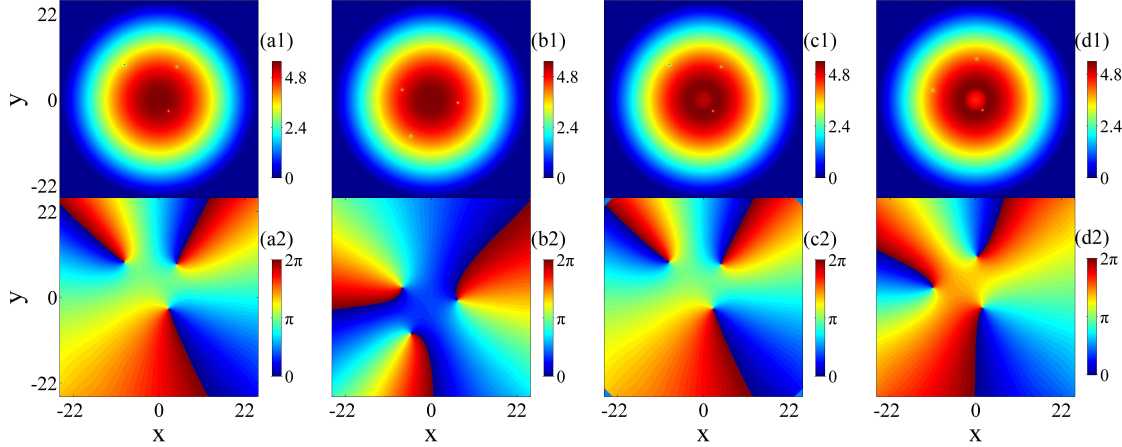


FIG. 6: The effects of the boson-fermion interactions on the vortex-lattice formations in the slowly rotating Fermi superfluid, for the relatively small strengths: (a) $\tilde{a}_{bf} = 0.01$, (b) 0.05, (c) 0.5, and (d) 1. The rotation frequency is fixed to be $\Omega = 0.05\omega_{f\perp}$. Shown in upper panels (a1)-(d1) are the cross-sectional densities (in units of 10^{-4}) at $z = 0$ plane, and lower panels (a2)-(d2) are the corresponding cross-sectional phases.

In the first experiment on producing coupled vortex lattices in the Bose-Fermi superfluid mixtures [31], it was detected that the repulsive boson-fermion interaction leads to prominent increase of the vortex number in the Fermi superfluid, while it has less effects on the vortex number of the Bose superfluid. Here we start from a very small value of the rotation frequency, and examine the effect of the boson-fermion interaction on the vortex nucleation. We first illustrate our results in Fig. 6 for the Fermi superfluids with a very small rotation frequency $\Omega = 0.05\omega_{f\perp}$. It is found that even in the presence of a very weak boson-fermion strength $\tilde{a}_{bf} = 0.01$, one extra vortex emerges instantaneously as shown in Fig. 6(a). Comparing with the positions of the two vortices in the single Fermi superfluid (Fig. 1(a)), such negligible boson-fermion interaction also affects the vortex configurations. By further increasing from $\tilde{a}_{bf} = 0.05$ to 1 in Fig. 6(b)-(d), the vortex number keeps invariant. But

the density profile evolves into a configuration in which the central density becomes more depressed, the three vortices are attracted spirally to the center areas, which can be seen more clearly from the corresponding phases (Fig. 6(b2)-(d2)). In the experimental relevant Bose-Fermi system, the masses and the trap frequencies for bosons and fermions are both not equal. The rotation frequency is $\Omega = 0.05\omega_{f\perp} = 0.1\omega_{b\perp}$ as $\omega_{f\perp}/\omega_{b\perp} = 2$, which is thus much smaller than the critical frequency $0.5\omega_{b\perp}$, and the Bose superfluids without vortex nucleation like nonrotation are not shown here.

In addition, we find that the boson-fermion interaction decreases the critical frequency of the Fermi superfluid slightly from $\Omega_c = 0.0325\omega_{f\perp}$ to $0.031\omega_{f\perp}$. For $\Omega = 0.031\omega_{f\perp}$, a single vortex enters into the Fermi superfluid instantaneously when a very weak boson-fermion interaction is turned on. Our numerical result is consistent with the experimental finding that the interspecies interaction can result in the unexpected vortex formation in the Fermi superfluid and increase the vortex number.

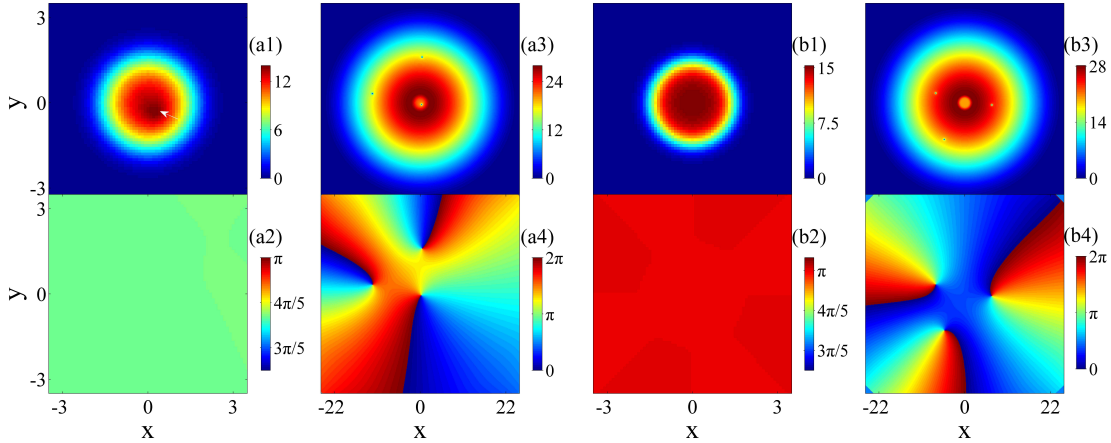


FIG. 7: Vortex-lattice structures in the slowly rotating Bose-Fermi superfluid mixtures in the immiscible regime for (a) $\tilde{a}_{bf} = 4$ and (b) 6. The rotation frequency is fixed to be $\Omega = 0.05\omega_{f\perp}$. Upper panels (a1) and (b1) show the integrated densities of the Bose superfluid $\int n_b(x, y, z)dz$ (in units of 10^{-2}), and (a3) and (b3) show the integrated densities of the Fermi superfluid $\int n_f(x, y, z)dz$ (in units of 10^{-4}). Lower panels are the corresponding cross-sectional phases.

In Fig. 7 we show the same case of Fig. 6 in the immiscible regime. For $\tilde{a}_{bf} = 4$, the formation of the coreless vortex is observed with a vortex in the Fermi superfluid attracted

in the overlapping center area (Fig. 7(a3)), which creates a corresponding density peak in the Bose superfluid shown as a dark spot in Fig. 7(a1) denoted by the arrow. However, in Fig. 7(b) for a larger value $\tilde{a}_{bf} = 6$ where the Bose and Fermi superfluids are well separated, the coreless vortex disappears as the vortex is repelled from the overlapping center area. Instead of the cross-sectional densities in Fig. 6, we present the integrated densities along the z direction in the upper panels of Fig. 7. It is because that the cross-sectional density of the Fermi superfluid at the center is zero and the vortex is invisible. Note that the coreless vortex was first experimentally created in the two-component BEC [33]. In terms of a pseudospin representation [36], an axisymmetric vortex is interpreted as skyrmions, in which the vortex core of one component is filled with the other nonrotating component, while a nonaxisymmetric one is regarded as meron pairs, in which each component has one off-centered vortex [77]. Our results indicate that an axisymmetric structure of the coreless vortex states can be observed in the slowly rotating Bose-Fermi superfluid mixtures around the miscible-immiscible transition.

As the rotation frequency continues to increase above the threshold for the appearance of the first vortex in the Bose superfluid, we can study the interplay between the emerging vortex lattices in two components through the boson-fermion interaction. We find that a very weak interspecies interaction can lead to the first vortex of the Bose superfluid at $\Omega_c = 0.45\omega_{b\perp}$, which is unexpected for a single Bose superfluid with $\Omega_c = 0.5\omega_{b\perp}$.

In Fig. 8 we study the variations of vortex-lattice structures in the rapidly rotating Bose-Fermi superfluid mixtures ($\Omega = 0.35\omega_{f\perp}$) in the miscible regime as a function of the interspecies interaction. In the absence of the interaction $\tilde{a}_{bf} = 0$ in Fig. 8(a), the Bose and Fermi superfluids behave independently and the vortex lattices in two superfluids are uncoupled. With the onset of a very weak boson-fermion interaction $\tilde{a}_{bf} = 0.05$, one extra vortex appears immediately in the Bose superfluid as shown in Fig. 8(b1), and the vortex number increases from three to four. The interspecies interaction also affects the arrangement of the vortices in the Fermi superfluid, which distribute from the center spirally to more regularly in Fig. 8(b3). With increasing the interaction $\tilde{a}_{bf} = 1$ in Fig. 8(c), the vortex number of the Bose superfluid keeps invariant. However, in Fig. 8(d) for $\tilde{a}_{bf} = 2$, we observe the annihilation of the vortex lattice in the Bose superfluid, in which one vortex disappears and three vortices are visible. For a larger strength $\tilde{a}_{bf} = 3$ in Fig. 8(e), only two visible vortices are left, despite it is still in the miscible phase.

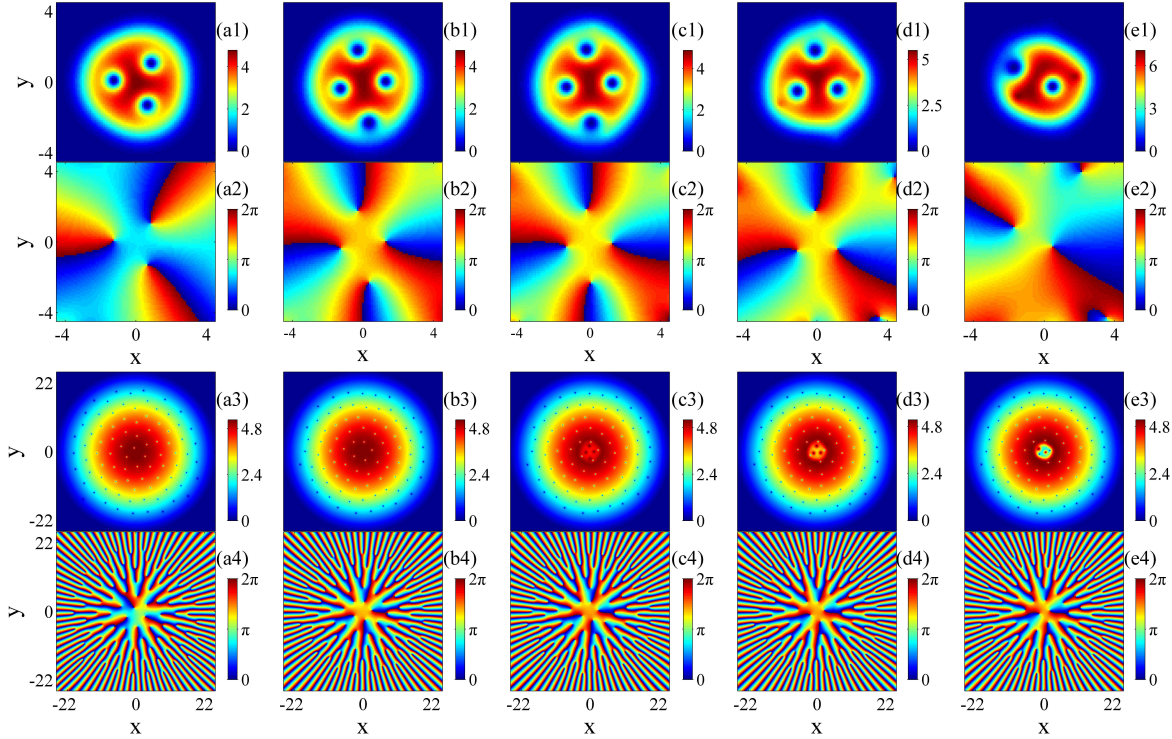


FIG. 8: Vortex-lattice structures in the fast rotating Bose-Fermi superfluid mixtures in the miscible regime, for (a) $\tilde{a}_{bf} = 0$, (b) 0.05, (c) 1.0, (d) 2.0 and (e) 3.0. The rotation frequency is fixed to be $\Omega = 0.35\omega_{f\perp}$. Panels (a1)-(e1) show the cross-sectional densities (in units of 10^{-2}) of the Bose superfluid at $z = 0$ plane, and (a3)-(e3) show the cross-sectional densities (in units of 10^{-4}) of the Fermi superfluid at $z = 0$ plane. Panels (a2)-(e2) and (a4)-(e4) are the corresponding cross-sectional phases.

This may explains the unconventional behaviors of the vortex number of the Bose superfluids due to the boson-fermion interaction observed in the experiment. In contrast to the Fermi superfluid, the boson-fermion interaction has less impact on the vortex number of the Bose superfluid, see Fig. 4 of Ref. [31]. More vortices are detected in the experiment than our numerical results. This is because the total numbers of bosons and fermions we use are an order of magnitude smaller than the experiment. The larger numbers of particles can result in the nucleation of more vortices, and enhance the miscible-immiscible transition, that is $\tilde{a}_{bf}^c = 2.8$ calculated from Eq. (10).

The numerical results for the same case of Fig. 8 in the immiscible regime are presented in Fig. 9. For $\tilde{a}_{bf} = 4$, there is no visible vortex left in the Bose superfluid as shown

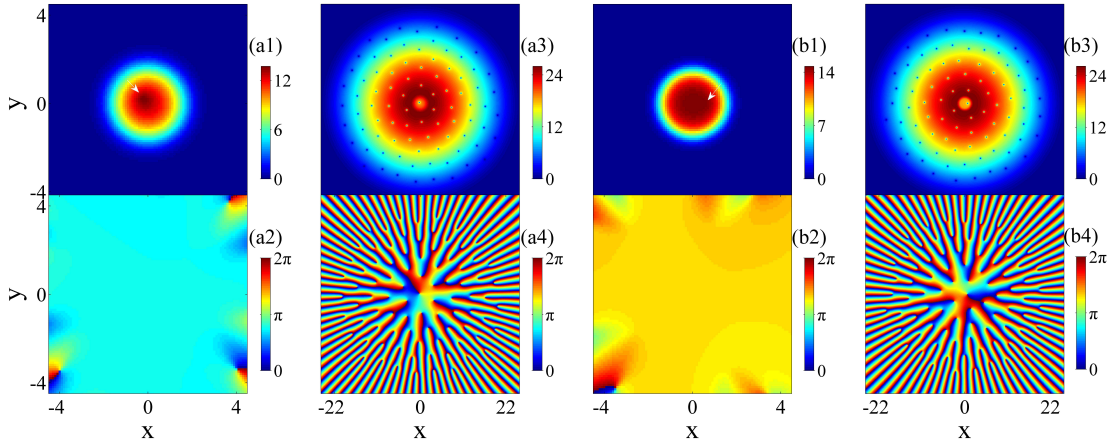


FIG. 9: The same case as Fig. 8 in the immiscible regime for (a) $\tilde{a}_{bf} = 4$ and (b) 6. Upper panels (a1) and (b1) show the integrated densities of the Bose superfluid $\int n_b(x, y, z) dz$ (in units of 10^{-2}), and (a3) and (b3) show the integrated densities of the Fermi superfluid $\int n_f(x, y, z) dz$ (in units of 10^{-4}). Lower panels are the corresponding cross-sectional phases.

in Fig. 9(a1), and the vortex-lattice structure is also featured by a coreless vortex similar to Fig. 7(a) for a slowly rotating mixture. However, different from the disappearance of the coreless vortex under the slow rotation, the coreless vortex denoted by the arrow in Fig. 9(b1) still remains in the phase-separated state ($\tilde{a}_{bf} = 6$). The reason is that as the rotation frequency increases, more vortices in the Fermi superfluid prevent the vortex from leaving from the overlapping area shown in Fig. 9(b3).

Fig. 5 also shows the behavior of the miscibility of the rotating Bose-Fermi superfluid mixtures as a function of the boson-fermion interaction. One can find that the miscibility of the rotating mixtures enhances due to the centrifugal force, and increases with the rotation frequency. In addition, as the interspecies interaction increases, the discrepancies of the miscibility for different rotation frequencies in the phase-separated regime are narrowed.

We further consider the rotation frequency $\Omega = 0.45\omega_{f\perp}$ in Fig. 10 to study the coupling between the two superfluids containing more vortices. Interestingly, we find different features, except for one extra vortex emerging in the presence of a very weak interaction ($\tilde{a}_{bf} = 0.05$) in Fig. 10(b1) compared to Fig. 10(a1). As the boson-fermion interaction increases in Fig. 10(c)-10(e), the vortex lattice in the Bose superfluid annihilates with a de-

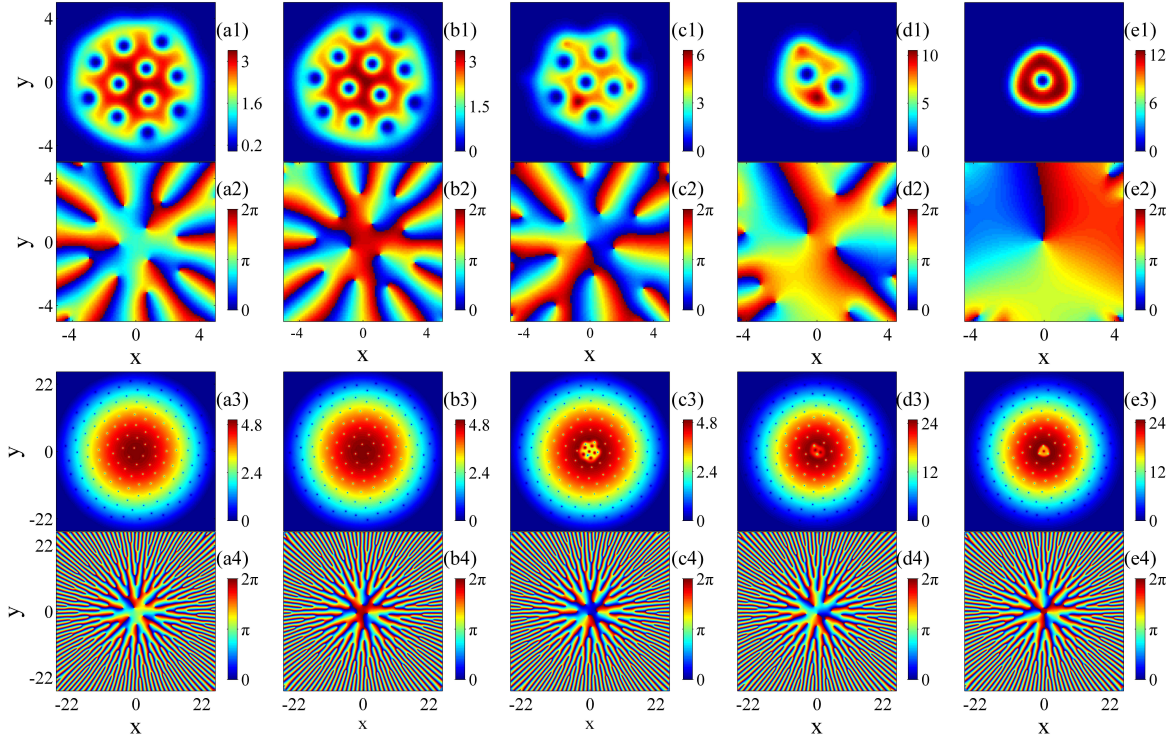


FIG. 10: Vortex-lattice structures in the fast rotating Bose-Fermi superfluid mixtures ($\Omega = 0.45\omega_{f\perp}$) for (a) $\tilde{a}_{bf} = 0$, (b) 0.05, and (c) 3.0 in the miscible regime, and (d) 4.0 and (e) 6.0 in the immiscible regime. Panels (a1)-(c1) show the cross-sectional densities (in units of 10^{-2}) of the Bose superfluid at $z = 0$ plane, and (a3)-(c3) show the cross-sectional densities (in units of 10^{-4}) of the Fermi superfluid at $z = 0$ plane. In contrast, shown in (d1) and (e1) are the integrated densities (in units of 10^{-2}) of the Bose superfluid, and (d3) and (e3) are the integrated densities (in units of 10^{-4}) of the Fermi superfluid. Panels (a2)-(e2) and (a4)-(e4) correspond to the cross-sectional phases of the Bose superfluid and the Fermi superfluid, respectively.

crease of the vortex number. However, instead of the coreless vortex in the phase-separated state ($\tilde{a}_{bf} = 6$) observed before, the vortex lattice is featured by a new structure as shown in Fig. 10(e). It is seen that a single vortex in the Bose superfluid remains at the center (Fig. 10(e1)), which can be verified by the corresponding phase (Fig. 10(e2)). This vortex is surrounded by three nearest-neighbor vortices in the Fermi superfluid (Fig. 10(e3)) locating at three vertices of the resultant triangular boundary of the Bose superfluid. Moreover, we plot 3D visualization of the new structure in Fig. 11(b). It is seen that the vortex lines in the Fermi superfluid pass through the Bose superfluid, bending towards to the vortex of the Bose

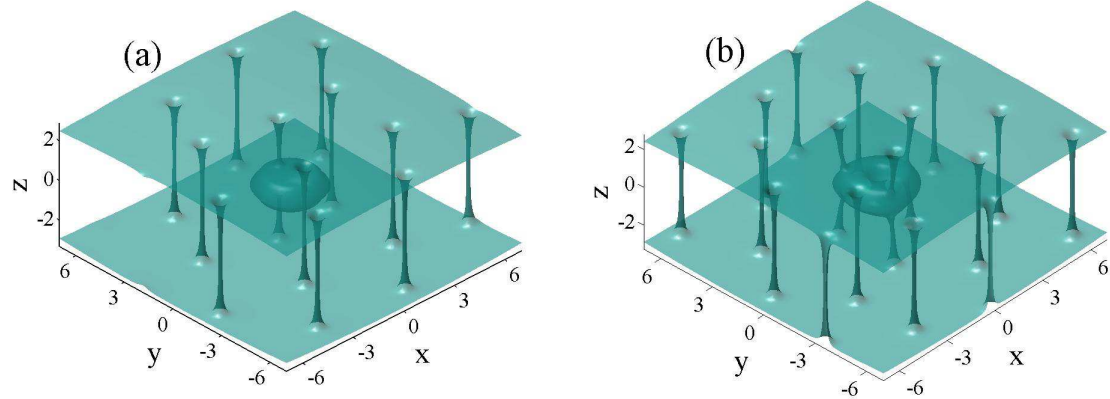


FIG. 11: Closeup of 3D visualization (isosurface plot at 1.6×10^{-4}) of the vortex-lattice structures in the phase-separated state. (a) $\Omega = 0.35\omega_{f\perp}$ and (b) $0.45\omega_{f\perp}$.

superfluid featured by a hole at the center, which implies attractive interactions between two vortices of these two different superfluids. The bending of the straight vortex lines in turn leads to the triangular shape of the Bose superfluid. For comparison, we also plot 3D visualization of the coreless vortex in Fig. 11(a), which is characterized by a straight vortex line of the Fermi superfluid across the vortex-free Bose superfluid without any deformation.

V. CONCLUSIONS

We have revealed the equilibrium structures of the rotating oblate Bose-Fermi superfluid mixtures in the unitary limit by varying the rotation frequency and the repulsive boson-fermion interaction. In contrast to the well-known rotating two-component BECs, such a $^{41}\text{K}-^6\text{Li}$ boson-fermion mixture is a highly asymmetric system, with unequal masses, particle numbers, trapping frequencies, and intraspecies interactions. The critical frequency of the first vortex nucleation in the weakly interacting Bose superfluid is $\Omega_c = 0.5\omega_{b\perp} = 0.25\omega_{f\perp}$, while the strongly interacting Fermi superfluid with one order of magnitude more particles than the Bose superfluid has a much smaller critical frequency $\Omega_c = 0.0325\omega_{f\perp}$. In the very slowly rotating regimes below the critical frequency of the Bose superfluid, it is clearly that one more vortex can emerge in the Fermi superfluid immediately, when a very small

repulsive boson-fermion interaction is turned on. The vortex number remains unchanged as the repulsive boson-fermion interaction increases, but the vortex configuration is affected with the vortices moving spirally to the overlapping center area. Nearby the miscible-immiscible transition, one axisymmetric coreless vortex forms in the center area in that the vortex core of the Fermi superfluid is filled with the nonrotating Bose superfluid. In the phase-separated state, the coreless vortex disappears as the vortex in the Fermi superfluid leaves from the overlapping center area. In the fast rotating regimes, a very small repulsive boson-fermion interaction can also lead to one extra vortex emerging in the Bose superfluid. However, with the increase of the repulsive boson-fermion interaction, the vortex lattices annihilate with a decrease of the vortex number and the vortex-lattice structure in the phase-separated state is finally featured by the coreless vortex. By further increasing the rotation frequency, the vortex lattice in the phase-separated state is characterized by a new structure. Instead of the coreless vortex, the single remaining vortex in the Bose superfluid is surrounded by the three vortices in the Fermi superfluid in the overlapping area. The 3D visualization of the new vortex state indicates the attractive interactions between two vortices of these two superfluids. This study not only provides insight into rich phenomena that emerge in the rotating Bose-Fermi superfluid mixture, but also sheds light on the unconventional behaviors of the vortex numbers arising from the interplay between Bose and Fermi superfluidity observed in the experiment.

It should be noted that vortex lattices in strongly interacting Fermi superfluids cannot be resolved *in situ*, but detected after ramping the magnetic field to the BEC regime and performing time-flight imaging [17, 31]. The target value of the magnetic field, rate of the ramping, as well as expansion time after the release may impact the configurations of vortex lattices in the final state. A natural extension of this work would be to study how these parameters affect the expansions of a rotating strongly interacting Fermi superfluid by using a orbital-free DFT with dissipation [27, 78, 79].

Acknowledgments

We thank Han Pu for stimulating this work, and Linhua Wen, Peng Zou and Xiang-Pei Liu for insightful discussions. This work is supported by the National Natural Science Foundation of China (NSFC) (Grant No. 12074343, No. 12074120, and No. 11374003)

and Natural Science Foundation of Shanghai (Grant No. 20ZR1418500). The numerical calculations in this paper have been done on the Tianhe-2 supercomputing system in the national supercomputer center in Guangzhou.

- [1] C. J. Pethick and H. Smith, *Bose-Einstein Condensation in Dilute Gases*, 2nd ed. (Cambridge University Press, New York, 2008).
- [2] A. L. Fetter and A. A. Svidzinsky, Vortices in a trapped dilute Bose-Einstein condensate, *J. Phys.: Condens. Matter* **13**, R135 (2001).
- [3] A. L. Fetter, Rotating trapped Bose-Einstein condensates, *Rev. Mod. Phys.* **81**, 647 (2009).
- [4] J. R. Abo-Shaeer, C. Raman, J. M. Vogels, and W. Ketterle, Observation of vortex lattices in Bose-Einstein condensates, *Science* **292**, 476 (2001).
- [5] K. W. Madison, F. Chevy, W. Wohlleben, and J. Dalibard, Vortex formation in a stirred Bose-Einstein condensate, *Phys. Rev. Lett.* **84**, 806 (2000).
- [6] D. L. Feder and C. W. Clark, Superfluid-to-solid crossover in a rotating Bose-Einstein condensate, *Phys. Rev. Lett.* **87**, 190401 (2001).
- [7] M. Tsubota, K. Kasamatsu, and M. Ueda, Vortex lattice formation in a rotating Bose-Einstein condensate, *Phys. Rev. A* **65**, 023603 (2002).
- [8] C. Lobo, A. Sinatra, and Y. Castin, Vortex lattice formation in Bose-Einstein condensates, *Phys. Rev. Lett.* **92**, 020403 (2004).
- [9] I. Bloch, J. Dalibard, and W. Zwerger, Many-body physics with ultracold gases, *Rev. Mod. Phys.* **80**, 885 (2008).
- [10] W. Zwerger (Ed.), *The BCS-BEC Crossover and the Unitary Fermi Gas (Lecture Notes in Physics vol 836)*, (Springer, Berlin, 2012).
- [11] G. D. Pace, K. Xhani, A. M. Falconi, M. Fedrizzi, N. Grani, D. H. Rajkov, M. Inguscio, F. Scazza, W. J. Kwon, and G. Roati, Imprinting persistent currents in tunable fermionic rings, arXiv:2204.06542 v2 (2022).
- [12] Y. Cai, D. G. Allman, P. Sabharwal, and K. C. Wright, Persistent currents in rings of ultracold fermionic atoms, *Phys. Rev. Lett.* **128**, 150401 (2022).
- [13] X.-P. Liu, X.-C. Yao, Y. Deng, Y.-X. Wang, X.-Q. Wang, X. Li, Q. Chen, Y.-A. Chen, and J.-W. Pan, Dynamic formation of quasicondensate and spontaneous vortices in a strongly

interacting Fermi gas, Phys. Rev. Research **3**, 043115 (2021).

[14] F. Li, S. Deng, L. Zhang, J. Xia, L. Yi, and H. Wu, Light induced space-time patterns in a superfluid Fermi gas, Sci. China-Phys. Mech. Astron. **64**, 294212 (2021).

[15] D. H.-Rajkov, J. E. P.-Castillo, A. d. R.-Lima, A. G.-Valdés, F. J. P.-Cuevas and J. A. Seman, Faraday waves in strongly interacting superfluids, New J. Phys. **23**, 103038 (2021).

[16] M. W. Zwierlein, J. R. A.-Shaeer, A. Schirotzek, C. H. Schunck, and W. Ketterle, Vortices and superfluidity in a strongly interacting Fermi gas, Nature **435**, 1047 (2005).

[17] C. H. Schunck, M. W. Zwierlein, A. Schirotzek, and W. Ketterle, Superfluid expansion of a rotating Fermi gas, Phys. Rev. Lett. **98**, 050404 (2007).

[18] S. Giorgini, L. P. Pitaevskii and S. Stringari, Theory of ultracold atomic Fermi gases, Rev. Mod. Phys. **80**, 1215 (2008).

[19] A. Bulgac, M. M. Forbes, and P. Magierski, The unitary Fermi gas: From Monte Carlo to density functionals, in *The BCS-BEC Crossover and the Unitary Fermi Gas*, edited by W. Zwerger (Springer, Berlin, 2012).

[20] D. L. Feder, Vortex arrays in a rotating superfluid Fermi gas, Phys. Rev. Lett. **93**, 200406 (2004).

[21] S. Simonucci, P. Pieri, and G. C. Strinati, Vortex arrays in neutral trapped Fermi gases through the BCS-BEC crossover, Nat. Phys. **11**, 941 (2015).

[22] H. Hu and X.-J. Liu, Density fingerprint of giant vortices in Fermi gases near a Feshbach resonance, Phys. Rev. A **75**, 011603(R) (2007).

[23] L. Kong, G. Fan, S.-G. Peng, X.-L. Chen, H. Zhao, and P. Zou, Dynamical generation of solitons in one-dimensional Fermi superfluids with and without spin-orbit coupling, Phys. Rev. A **103**, 063318 (2021).

[24] A. Bulgac and Y. Yu, Vortex state in a strongly coupled dilute atomic fermionic superfluid, Phys. Rev. Lett. **91**, 190404 (2003).

[25] A. Bulgac, Y.-L. Luo, P. Magierski, K. J. Roche, and Y. Yu, Real-time dynamics of quantized vortices in a unitary Fermi superfluid, Science **332**, 1288 (2011).

[26] A. Bulgac, M. M. Forbes, M. M. Kelley, K. J. Roche, and G. Wlazłowski, Quantized superfluid vortex rings in the unitary Fermi gas, Phys. Rev. Lett. **112**, 025301 (2014).

[27] K. Hossain, K. Kobuszewski, M. M. Forbes, P. Magierski, K. Sekizawa, and G. Wlazłowski, Rotating quantum turbulence in the unitary Fermi gas, Phys. Rev. A **105**, 013304 (2022).

[28] J. Kopyciński, W. R. Pudelko, and G. Włazłowski, Vortex lattice in spin-imbalanced unitary Fermi gas, *Phys. Rev. A* **104**, 053322 (2021).

[29] I. F.-Barbut, M. Delehaye, S. Laurent, A. T. Grier, M. Pierce, B. S. Rem, F. Chevy, and C. Salomon, A mixture of Bose and Fermi superfluids, *Science* **345**, 1035 (2014).

[30] T. Ikemachi, A. Ito, Y. Aratake, Y. Chen, M. Koashi, M. K.-Gonokami and M. Horikoshi, All-optical production of dual Bose-Einstein condensates of paired fermions and bosons with ^6Li and ^7Li , *J. Phys. B: At. Mol. Opt. Phys.* **50**, 01LT01 (2017).

[31] X.-C. Yao, H.-Z. Chen, Y.-P. Wu, X.-P. Liu, X.-Q. Wang, X. Jiang, Y. Deng, Y.-A. Chen, and J.-W. Pan, Observation of coupled vortex lattices in a mass-imbalance Bose and Fermi superfluid mixture, *Phys. Rev. Lett.* **117**, 145301 (2016).

[32] R. Roy, A. Green, R. Bowler, and S. Gupta, Two-element mixture of Bose and Fermi superfluids, *Phys. Rev. Lett.* **118**, 055301 (2017).

[33] M. R. Matthews, B. P. Anderson, P. C. Haljan, D. S. Hall, C. E. Wieman, and E. A. Cornell, Vortices in a Bose-Einstein condensate, *Phys. Rev. Lett.* **83**, 2498 (1999).

[34] B. P. Anderson, P. C. Haljan, C. E. Wieman, and E. A. Cornell, Vortex precession in Bose-Einstein condensates: obervations with filled and empty cores, *Phys. Rev. Lett.* **85**, 2857 (2000).

[35] V. Schweikhard, I. Coddington, P. Engels, S. Tung, and E. A. Cornell, Vortex-lattice dynamics in rotating spinor Bose-Einstein condensates, *Phys. Rev. Lett.* **93**, 210403 (2004).

[36] K. Kasamatsu, M. Tsubota, and M. Ueda, Vortices in multicomponent Bose-Einstein condensates, *Int. J. Mod. Phys. B* **19**, 1835 (2005).

[37] H. Pu and N. P. Bigelow, Properties of two-species Bose condensates, *Phys. Rev. Lett.* **80**, 1130 (1998).

[38] E. J. Mueller and T. L. Ho, Two-component Bose-Einstein condensates with a large number of vortices, *Phys. Rev. Lett.* **88**, 180403 (2002).

[39] K. Kasamatsu, M. Tsubota, and M. Ueda, Vortex phase diagram in rotating two-component Bose-Einstein condensate, *Phys. Rev. Lett.* **91**, 150406 (2003);

[40] K. Kasamatsu and M. Tsubota, Vortex sheet in rotating two-component Bose-Einstein condensates, *Phys. Rev. A* **79**, 023606 (2009).

[41] K. Kasamatsu and K. Sakashita, Stripes and honeycomb lattice of quantized vortices in rotating two-component Bose-Einstein condensates, *Phys. Rev. A* **97**, 053622 (2018).

[42] P. Mason and A. Aftalion, Classification of the ground states and topological defects in a rotating two-component Bose-Einstein condensate, *Phys. Rev. A* **84**, 033611 (2011).

[43] A. Aftalion, P. Mason, and J. Wei, Vortex-peak interaction and lattice shape in rotating two-component Bose-Einstein condensates, *Phys. Rev. A* **85**, 033614 (2012).

[44] S. K. Adhikari, Phase-separated symmetry-breaking vortex-lattice in a binary Bose-Einstein condensate, *Physica E* **115**, 113713 (2020).

[45] L. Mingarelli and R. Barnett, Exotic vortex lattices in binary repulsive superfluids, *Phys. Rev. Lett.* **122**, 045301 (2019).

[46] L. Mingarelli, E. E. Keaveny and R. Barnett, Vortex lattices in binary mixtures of repulsive superfluids, *Phys. Rev. A* **97**, 043622 (2018).

[47] L. Wen and J. Li, Structure of dynamics of a rotating superfluid Bose-Fermi mixture, *Phys. Rev. A* **90**, 053621 (2014).

[48] Y. Jiang, R. Qi, Z.-Y. Shi, and H. Zhai, Vortex lattices in the Bose-Fermi superfluid mixture, *Phys. Rev. Lett.* **118**, 080403 (2017).

[49] J.-S. Pan, W. Zhang, W. Yi and G.-C. Guo, Vortex-core structure in a mixture of Bose and Fermi superfluids, *Phys. Rev. A* **95**, 063614 (2017).

[50] M. Ögren and G. M. Kavoulakis, Rotational properties of superfluid Fermi-Bose mixtures in a tight torodial trap, *Phys. Rev. A* **102**, 013323 (2020).

[51] Y. E. Kim and A. L. Zubarev, Time-dependent density-functional theory for trapped strongly interacting fermionic atoms, *Phys. Rev. A* **70**, 033612 (2004).

[52] L. Salasnich, N. Manini, and F. Toigo, Macroscopic periodic tunneling of Fermi atoms in the BCS-BEC crossover, *Phys. Rev. A* **77**, 043609 (2008).

[53] L. Salasnich and F. Toigo, Extended Thomas-Fermi density functional for the unitary Fermi gas, *Phys. Rev. A* **78**, 053626 (2008).

[54] S. K. Adhikari, Nonlinear Schrödinger equation for a superfluid Fermi gas in the BCS-BEC crossover, *Phys. Rev. A* **77**, 045602 (2008).

[55] W. Wen, Y. Zhou, and G. Huang, Interference patterns of superfluid Fermi gases in the BCS-BEC crossover released from optical lattices, *Phys. Rev. A* **77**, 033623 (2008).

[56] S. K. Adhikari and L. Salasnich, Superfluid Bose-Fermi mixture from weak coupling to unitarity, *Phys. Rev. A* **78**, 043616 (2008).

[57] S. K. Adhikari, B. A. Malomed, L. Salasnich, and F. Toigo, Spontaneous symmetry breaking

of Bose-Fermi mixtures in double-well potentials, *Phys. Rev. A* **81**, 053630 (2010).

[58] Y. Cheng and S. K. Adhikari, Localization of a Bose-Fermi mixture in a bichromatic optical lattice, *Phys. Rev. A* **84**, 023632 (2011).

[59] W. Wen and H.-j. Li, Collective dipole oscillations in a mixture of Bose and Fermi superfluids in the BCS-BEC crossover, *New J. Phys.* **20**, 083044 (2018).

[60] K. Hossain, S. Gupta, and M. M. Forbes, Detecting entrainment in Fermi-Bose mixtures, *Phys. Rev. A* **105**, 063315 (2022).

[61] A. J. Leggett, *Quantum Liquids: Bose Condensation and Cooper Pairing in Condensed Matter Systems* (Oxford University Press, Oxford, 2006).

[62] M. M. Forbes and R. Sharma, Validating simple dynamical simulations of the unitary Fermi gas, *Phys. Rev. A* **90**, 043638 (2014).

[63] W. Wen, C. Zhao and X. Ma, Dark-soliton dynamics and snake instability in superfluid Fermi gases trapped by an anisotropic harmonic potential, *Phys. Rev. A* **88**, 063621 (2013).

[64] N. Navon, S. Nascimbène, F. Chevy, and C. Salomon, The equation of state of a low-temperature Fermi gas with tunable interactions, *Science* **328**, 729 (2010).

[65] N. Manini and L. Salasnich, Bulk and collective properties of a dilute Fermi gas in the BCS-BEC crossover, *Phys. Rev. A* **71**, 033625 (2005).

[66] W. Wen, S.-Q. Shen, and G. Huang, Propagation of sound and supersonic bright solitons in superfluid Fermi gases in BCS-BEC crossover, *Phys. Rev. B* **81**, 014528 (2010).

[67] R. K. Kumar, V. Lončar, P. Muruganandam, S. K. Adhikari, and A. Balaž, C and Fortran OpenMP programs for rotating Bose-Einstein condensates, *Comput. Phys. Commun.* **240**, 74 (2019).

[68] R. K. Kumar, L. Tomio, B. A. Malomed, and A. Gammal, Vortex lattices in binary Bose-Einstein condensates with dipole-dipole interactions, *Phys. Rev. A* **96**, 063624 (2017).

[69] P. Muruganandam and S. K. Adhikari, Fortran programs for the time-dependent Gross-Pitaevskii equation in a fully anisotropic trap, *Comput. Phys. Commun.* **180**, 1888 (2009).

[70] B. Satarić, V. Slavnić, A. Belić, A. Balaž, P. Muruganandam, and S. K. Adhikari, Hybrid OpenMP/MPI programs for solving the time-dependent Gross-Pitaevskii equation in a fully anisotropic trap, *Comput. Phys. Commun.* **200**, 411 (2016).

[71] R. P. Feynman, in *Progress in Low Temperature Physics*, edited by C. J. Gorter (North-Holland, Amsterdam, 1955), Chap. 2.

- [72] L. Zhang, W. Wen, J. Qian, X. Ma and Y. Wang, Anisotropic expansions of a strongly interacting Fermi superfluid containing a vortex, *J. Phys. B: At. Mol. Opt. Phys.* **53**, 155304 (2020).
- [73] G. M. Brunn and L. Viverit, Vortex state in superfluid trapped Fermi gases at zero temperature, *Phys. Rev. A* **64**, 063606 (2001).
- [74] H. Zhai and T.-L. Ho, Critical rotational frequency for superfluid fermionic gases across a Feshbach resonance, *Phys. Rev. Lett.* **97**, 180414 (2006).
- [75] S. G. Bhongale and H. Pu, Phase separation in a mixture of a Bose-Einstein condensate and a two-component Fermi gas as a probe of Fermi superfluidity, *Phys. Rev. A* **78**, 061606(R) (2008).
- [76] L. Salasnich and F. Toigo, Fermi-Bose mixture across a Feshbach resonance, *Phys. Rev. A* **75**, 013623 (2007).
- [77] K. Kasamatsu, M. Tsubota, and M. Ueda, Spin textures in rotating two-component Bose-Einstein condensates, *Phys. Rev. A* **71**, 043611 (2005).
- [78] S. Choi, S. A. Morgan, and K. Burnett, Phenomenological damping in trapped atomic Bose-Einstein condensates, *Phys. Rev. A* **57**, 4057 (1998).
- [79] N. P. Proukakis and B. Jackson, Finite-temperature models of Bose-Einstein condensation, *J. Phys. B: At. Mol. Opt. Phys.* **41**, 203002 (2008).